Temporal dynamics of spontaneous MEG activity in brain networks

Francesco de Pasquale[a,b,1], Stefania Della Penna[a,b], Abraham Z. Snyder[c,d], Christopher Lewis[a,b], Dante Mantini[a,b,2], Laura Marzetti[a,b], Paolo Belardinelli[a,b], Luca Ciancetta[a,b], Vittorio Pizzella[a,b], Gian Luca Romani[a,b], and Maurizio Corbetta[a,b,c,d]

[a]Institute for Advanced Biomedical Technologies, G. D'Annunzio University Foundation, G. D'Annunzio University, 66100 Chieti, Italy; [b]Department of Clinical Sciences and Bio-imaging, G. D'Annunzio University, 66100 Chieti, Italy; [c]Department of Neurology, Washington University, St. Louis, MO 63110; and [d]Department of Radiology, Washington University, St. Louis, MO 63110

Edited by Marcus E. Raichle, Washington University, St. Louis, MO, and approved January 29, 2010 (received for review December 3, 2009)

Functional MRI (fMRI) studies have shown that low-frequency (<0.1 Hz) spontaneous fluctuations of the blood oxygenation level dependent (BOLD) signal during restful wakefulness are coherent within distributed large-scale cortical and subcortical networks (resting state networks, RSNs). The neuronal mechanisms underlying RSNs remain poorly understood. Here, we describe magnetoencephalographic correspondents of two well-characterized RSNs: the dorsal attention and the default mode networks. Seed-based correlation mapping was performed using time-dependent MEG power reconstructed at each voxel within the brain. The topography of RSNs computed on the basis of extended (5 min) epochs was similar to that observed with fMRI but confined to the same hemisphere as the seed region. Analyses taking into account the nonstationarity of MEG activity showed transient formation of more complete RSNs, including nodes in the contralateral hemisphere. Spectral analysis indicated that RSNs manifest in MEG as synchronous modulation of band-limited power primarily within the theta, alpha, and beta bands—that is, in frequencies slower than those associated with the local electrophysiological correlates of event-related BOLD responses.

resting state networks | default mode network | dorsal attention network | functional MRI

The existence of resting state networks (RSNs) is now a well-established fMRI phenomenon (1). The basic finding is that in awake, quietly resting humans, spontaneous, slow (<0.1 Hz) fluctuations of the blood oxygen level dependent (BOLD) signal are temporally coherent within widely distributed functional networks closely resembling those evoked by sensory, motor, and cognitive paradigms (2). Interindividual differences in RSN properties may correlate with cognitive abilities both in health (2) and disease (3). Thus, correlated spontaneous neural activity in distributed brain networks represents a fundamental aspect of brain physiology and psychology. Though there is significant evidence linking stimulus-evoked BOLD responses, activations and deactivations both (4), and changes in local field potential (LFP) power, especially in the gamma (40-160 Hz) band, data bearing on the electrophysiological correlates of RSNs are scarce. Recent electrocorticography (ECoG) recordings in human subjects have shown a relationship between the topography of a sensory-motor RSN and slow cortical potentials (5). Slow (~0.1 Hz) fluctuations of the band-limited gamma power have been also reported as an electrophysiological correlate of BOLD signal fluctuations between brain areas within (5, 6) and across hemispheres in both humans (7) and monkeys (8). Though invasive recordings of electrophysiological activity in animals (8) or humans undergoing surgical management of epilepsy (5, 7) provide high spatial and temporal resolution and specificity, they are not ideal for the study of large-scale RSN in healthy volunteers. Not only are these methods invasive, but recordings through grids or electrodes grids typically cover only a small fraction of the cortical surface. Here we explore magnetoencephalography (MEG) to study the electrophysiological correlates of RSNs. MEG noninvasively records from outside the scalp the magnetic field variations induced by synaptic currents, which is the same physiology underlying LFPs (9). Although the MEG spatial resolution is limited (on the order of several millimeters), and the method has a low signal to noise, it does offer millisecond-scale temporal resolution and, most importantly for RSN studies, whole-head coverage (9). We focus on the dorsal attention network (DAN) and the default mode network (DMN), two of the most robust and well-studied RSNs that have been associated opposed functionality (externally vs. internally oriented cognition, respectively) (10).

Results

Stationary fMRI and MEG Resting State Networks. Seed-based resting-state fMRI correlation maps of the DAN and DMN were generated as in ref. 11 by computing the conjunction voxel-wise of temporal correlation maps calculated using different seed regions (Table S1 and *SI Text*). Main regions of the DAN bilaterally include anterior and posterior intraparietal sulcus (pIPS), the intersection of precentral and superior frontal sulcus (human FEF), and the middle temporal area (MT; Fig. 1, fMRI). The main regions of the DMN include left and right angular gyrus (LAG, RAG), left precuneus/posterior cingulate (LPCC), anterior temporal, and left and right medial prefrontal cortex (L/R MPFC; Fig. 2, fMRI). The two networks are anticorrelated after removal of a global signal before seed-based correlation mapping (12). For the MEG analyses, we used a similar approach, computing correlation maps using source-space, wide-band (1-150 Hz) power time series. MEG correlation seeds were selected on the basis of fMRI (see *Materials and Methods* and *SI Text*). For the DAN, we observed significant local correlation near the seed (LpIPS) and distant correlation with other regions in the DAN of the same hemisphere, but not with regions in the opposite hemisphere or outside of the DAN. ANOVA of the Pearson's r over multiple regions of the DAN, localized by fMRI correlation mapping, showed statistically significant correlation only with left FEF ($P < 0.0001$) and left ventral IPS (LvIPS; $P < 0.000001$; Fig. 1, Stationary MEG). When the analysis was repeated with right pIPS as the seed, we obtained a similar topography with significant correlation in right FEF and right vIPS, but no correlation in the DAN left hemisphere or elsewhere in the brain (Fig. S1*A*). Interestingly, there was no evidence of negative correlation between DAN and DMN as seen in fMRI (13) (see discussion in *SI Text*).

Author contributions: F.d.P., S.D.P., A.Z.S., P.B., L.C., V.P., G.L.R., and M.C. designed research; S.D.P., A.Z.S., C.L., D.M., L.M., and M.C. performed research; F.d.P., S.D.P., A.Z.S., and M.C. contributed new reagents/analytic tools; F.d.P., S.D.P., and M.C. analyzed data; and F.d.P., S.D.P., and M.C. wrote the paper.

The authors declare no conflict of interest.

This article is a PNAS Direct Submission.

[1]To whom correspondence should be addressed. E-mail: f.depasquale@unich.it.

[2]Present address: Laboratory for Neuro-psychophysiology, K.U. Leuven Medical School, 3000 Louvain, Belgium.

This article contains supporting information online at www.pnas.org/cgi/content/full/0913863107/DCSupplemental.

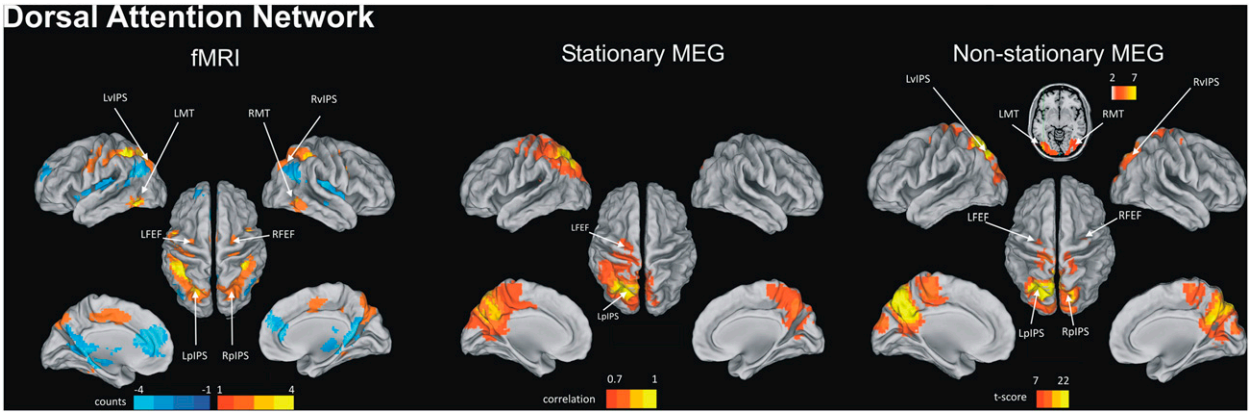

Fig. 1. Dorsal attention network. (*Left*) fMRI connectivity. A group conjunction map was obtained as in ref. 11 by combining voxel-wise individual temporal correlation maps of BOLD signal time series obtained from the four main nodes of the DAN (coordinates listed in Table S1). The map shows voxels with significant temporal correlation in at least three of four seeds. The represented quantity is seed count. (*Center*) Stationary MEG connectivity. Group average temporal correlation map of wide-band (1-150 Hz) power time-courses obtained from averaging individual temporal correlation maps obtained from seeding LpIPS, one of the core nodes of the DAN. The represented quantity is Pearson's *r*, and only values above the average correlation in the whole brain ($r = 0.7$) are displayed. (*Right*) Nonstationary MEG connectivity using MCW algorithm (seed, LpIPS; external node, RSFG). The represented quantity is a *t* statistic comparing voxelwise correlation with the seed vs. the mean correlation of the seed with the rest of the brain. pIPS, posterior intraparietal sulcus; FEF, frontal eye field; vIPS, ventral intraparietal sulcus; MT, middle temporal.

This pattern of intrahemispheric correlation cannot be explained by local blurring of signal due to volume conduction. First, although LvIPS is close to LpIPS [vector distance (VD) = 19 mm], FEF is farther away (VD = 55 mm), well within the spatial resolution of MEG. Second, we directly measured correlation along a trajectory connecting LpIPS to LFEF and found local minimum near the central sulcus (Fig. 1 and Fig. S1*B*).

We carried out a similar analysis for the DMN using LAG as the seed. Again we found significant correlation with other regions in the same hemisphere: left superior frontal sulcus (LSFS; $P < 0.05$), left posterior cingulate (LPCC; $P < 0.001$), and left retrosplenial cortex (LRS; $P < 0.001$), but not with homologous regions in the right hemisphere, or other regions outside the DMN (Fig. 2, Stationary MEG). Most of the regions of the DMN showing correlation with LAG were distant (LSFS, VD = 84 mm; LPCC, VD = 45 mm; RS, VD = 52 mm).

In summary, the topography of interregional MEG power correlation obtained under the assumption of temporal stationarity was similar to fMRI correlation maps in the hemisphere ipsilateral to the seed. However, robust interhemispheric correlation between homologous regions, as typically observed in resting state fMRI (14), was not observed in the MEG data. This discrepancy cannot be attributed to differences in temporal frequency content of the time series used for the correlation analyses. Convolution of the MEG power time series with a canonical hemodynamic response function (HRF) (15, 16) generated only a spatially blurred version of the original results (Fig. S1*C*).

Nonstationary MEG Resting State Networks. To investigate differences in RSN topography between MEG and fMRI, we examined the temporal dynamics of power fluctuations between various network nodes. Figure 3*A* shows prototypical MEG power time series from the four principal nodes of the DAN (L/R pIPS, L/R FEF) recorded over a 5-min run in one subject (Fig. 3*A*). Common fluctuations involving all four nodes can be discerned on a scale of minutes. However, on a finer temporal scale, it is apparent that periods of high correlation (e.g., between 10–20 s) alternate with periods of low correlation (e.g., between 208–218 s). This finding suggests that power fluctuations within a network are nonstationary.

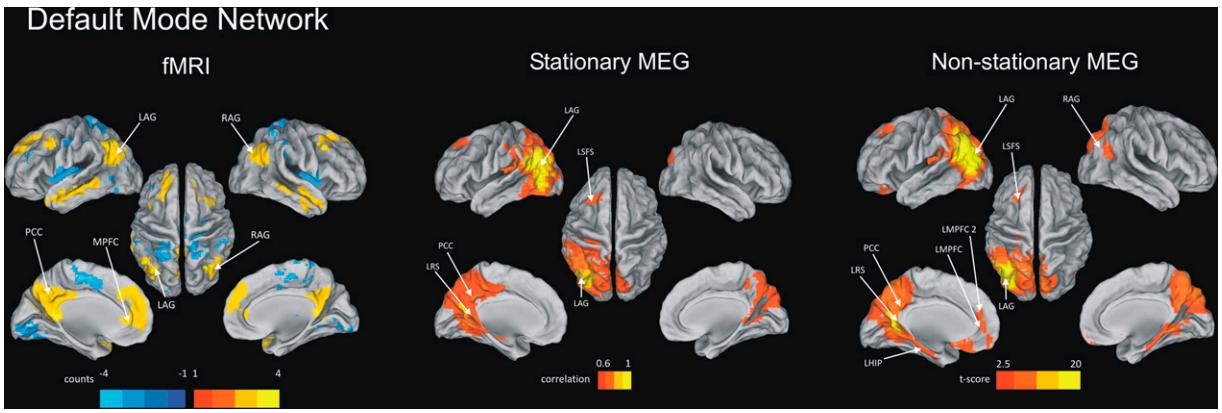

Fig. 2. Default mode network. (*Left*) fMRI conjunction maps obtained as in Fig. 1 corresponding to the DMN nodes. (*Center*) Stationary MEG connectivity obtained as in Fig. 1 (seed, LAG). Only values above the average correlation in the whole brain ($r = 0.6$) are reported. (*Right*) Nonstationary MEG connectivity using MCW algorithm (seed, LAG; external node, RSFG). L/R AG, angular gyrus; LPCC, left posterior cingulate cortex; L/R MPFC, medial prefrontal cortex; LRS, retrosplenial; L/R SFS, superior frontal sulcus; LHIP, left hippocampus.

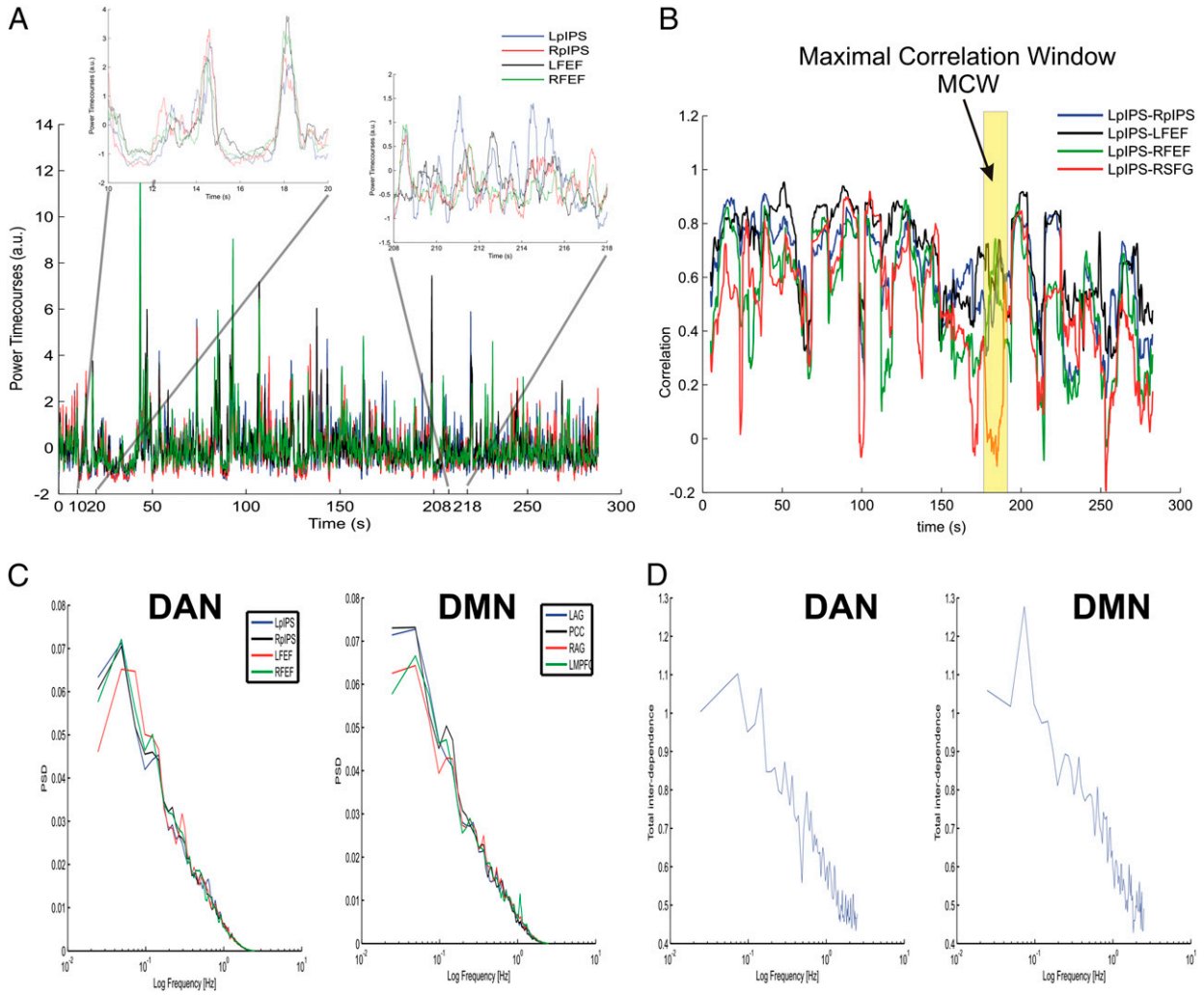

Fig. 3. (*A*) Wide-band MEG power time series (Eq. **2**) for the main nodes in the DAN (LpIPS, RpIPS, LFEF, and RFEF). (*B*) Correlation time series pairing LpIPS with other nodes in the DAN and one region outside of the DAN (RSFG). The represented quantity is $r_{sj}(t)$ (Eq. **3**; $T_r = 10$sec) evaluated at time increments of 0.2 s. (*C*) Power spectral densities (PSD) of wide-band power (Eq. **2**) in DAN and DMN nodes averaged across sessions and subjects. (*D*) Total interdependence measure (*SI Text*) for DAN and DMN on a semilog scale.

Figure 3*B* shows interregional correlation time series evaluated over a sliding 10-s window. An LpIPS seed is paired with other nodes within the DAN (RpIPS, L/R FEF), as well as with a region outside the DAN (right superior frontal gyrus, RSFG; Table S1). Regions within the DAN generally show stronger correlation than when LpIPS is paired with the external region. Again, intrahemispheric correlation (e.g., LpIPS-LFEF) is generally stronger than interhemispheric correlation (LpIPS-RFEF or LpIPS-RpIPS), as previously shown in the group-average correlation maps (Fig. 1). A critical feature evident in Fig. 3*B* is that MEG power time series interregional correlations fluctuate on a time scale on the order of tens of seconds, unlike BOLD interregional correlations, which are more stationary.

Based on these observations, we reasoned that nonstationarity may be responsible for the restricted intrahemispheric topography observed in MEG correlation maps, and thus more complete bilateral MEG networks will be observed on selected temporal epochs. To test this hypothesis, we examined the spectral properties of interregional correlations. Autospectra (Fig. 3*C*) and total interdependence, a measure of the internodal coherence (Fig. 3*D*, ref. 17, and *SI Text*), were computed for each subject on the principal nodes of the DAN (L/R pIPS; L/R FEF) and DMN (L/R AG; LPCC; LMPFC), and then averaged across subjects. Both measures displayed a 1/f-like spectral distribution, with the interdependence showing a moderate peak around 0.1 Hz for both DAN and DMN. Accordingly, 10 s (the reciprocal of 0.1 Hz) was chosen as the window duration for computing interregional power correlation (*SI Text*). To this aim, we developed the maximal correlation window (MCW) algorithm, which iteratively locates epochs in which the correlation between a seed region (e.g., LpIPS) and a subset of network nodes is high while, concurrently, the correlation with a region outside of the network is minimal (*Materials and Methods* and *SI Text*). An example of such temporal window is highlighted in yellow in Fig. 3*B*. The hypothesis is that other nodes within a network will be more coherent in temporal windows in which some of the component nodes show strong correlation. This procedure was applied to all 30 runs recorded in all 13 subjects. For each MCW, a whole-brain temporal correlation map was computed with the seed region. In each subject, maps derived from all MCWs were averaged, and a random effects statistical test assessed significance across subjects (*SI Text*).

The MEG power correlation map for the DAN computed using epochs selected by the MCW algorithm (seed, LpIPS; within-RSN nodes presented to the MCW algorithm, {RpIPS, LFEF, RFEF}; external node, RSFG) is shown in Fig. 1, Nonstationary MEG. Significant correlation was observed not only near the seed and

other nodes supplied to the MCW procedure, but also with several bilateral DAN regions (LMT, RMT, LvIPS, RvIPS) that were not used for epoch selection (Table S2, Dorsal Attention Network 1). The same regions also showed significant correlation when a different external node (LMPFC2) was used as control, hence when a different set of temporal windows was selected by the MCW algorithm (Fig. S2*A* and Table S2, Dorsal Attention Network 2).

A similar analysis assuming nonstationarity was conducted for the DMN (seed, LAG; within-network nodes presented to the MCW algorithm, {RAG, LPCC, LMPFC}; external node, RSFG or RFEF). Significant correlation was observed bilaterally in many DMN regions not used for epoch selection: left and right retrosplenial cortex (RS), left superior frontal sulcus (LSFS), right medial prefrontal cortex (RMPFC), left inferior temporal gyrus, and left hippocampus (LHIP) (Fig. 2, Nonstationary MEG; Fig. S2*B*; and Table S2, Default Mode Network 1 and 2). In general, MCW-selected epochs yielded MEG power time series correlations that were more bilateral and more similar to fMRI RSNs.

To assess the spatial similarity of MEG and fMRI results, a nonparametric test based on Spearman rank correlation as in ref. 5 compared covariance structures obtained by both methods. This test was applied to selected slices of the brain containing the principal nodes of each RSN (see *SI Text* for details). Significant correspondence ($P < 0.05$) was obtained in all subjects for each of the selected slices (for a representative result, see Fig. S3). Additional control analyses examined the variability of the nonstationary correlation within a network (Fig. S4*A*), the spatial specificity of the MCW maps (Fig. S4*B*), and verified that the MCW procedure did not artificially build RSNs (*SI Text* and Table S3).

Index of Network Correlation. The demonstration of nonstationary RSNs raises questions concerning network dynamics. As a preliminary analysis of this issue, the prevalence of within-network correlation was contrasted with the prevalence of across-network correlation. Thus, for a selected seed region, the index of network correlation quantified the fraction of epochs in which within-network correlation was significantly greater than the correlation with the external node (*Materials and Methods* and *SI Text*). The nodes were the same as those used in the MCW analysis. In both the DAN and the DMN (Fig. S4*C*), the seed was rarely (<10% of the time) more correlated with the external node than with each of the network nodes. In the DAN, significant correlation occurred the most frequently intrahemispherically (LpIPS-LFEF; index = 0.71); next, interhemispherically between homologous region pairs (LpIPS-RpIPS; index = 0.67); finally, least frequently, interhemispherically between nonhomologous regions (LpIPS-RFEF; index = 0.38). In other words, and notwithstanding nonstationarity, within-network correlation generally is greater than cross-network correlation. Thus, networks are always at least partially engaged. Within a network, intrahemispheric correlation is greater than interhemispheric correlation.

MEG RSN Dependence on Frequency Band. Previous ECoG studies (5, 7) and theoretical considerations (18) suggest that long-range and local synchronization are differentially reflected at low and high frequencies, respectively. To examine whether MEG RSNs depend on the frequency content of the signal, correlation mapping was performed with power restricted to the following bands: theta (3.5–7 Hz), alpha (8-13 Hz), beta (14-25 Hz), and gamma (27-70 Hz). In analyses assuming stationarity, band-limited topography for both the DAN and the DMN (Fig. S5) was generally similar for most frequencies to that obtained with wide-band power. However, no correlation extending outside the seed region was detected with power restricted to the gamma band. An ANOVA of correlation coefficients with band (theta, alpha, beta, gamma) as factor showed stronger correlation in alpha, and weaker correlation in gamma in both the DAN and the DMN (Fig. S6 *A* and *B*).

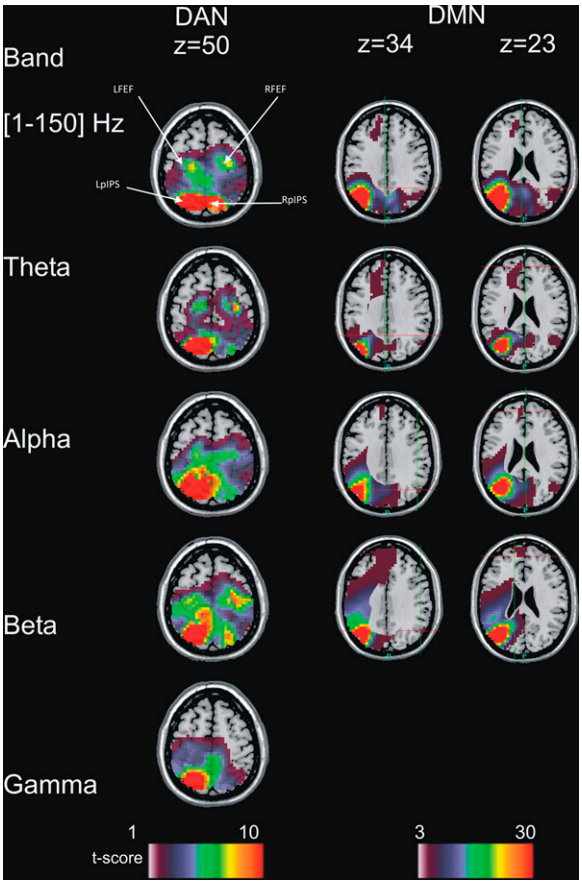

Fig. 4. Band-specific nonstationary MEG connectivity. (*Left*) Dorsal attention network (DAN; seed, LpIPS; external node, RSFG). The represented quantity is the *t* statistic as in Figs. 1 and 2 and one horizontal slice containing the main DAN nodes is shown ($z = 50$, MNI152). (*Right*) Default mode network (DMN, seed, LAG; external node, RSFG). Two horizontal slices containing the principal DMN nodes are shown ($z = 34$ and $z = 23$). No MCWs were identified in the gamma band for the DMN, indicating that this band contributes less to the connectivity than the others. The central part of the brain has been masked due to the limited accuracy of inverse source localization in that region.

In analyses of band-limited power correlation taking nonstationarity into account, sharper DAN topography (seed, LpIPS; external node, RSFG) was obtained with the theta and beta bands (Fig. 4), but the greatest significance at the group level (largest *t*-statistic values) was obtained in the alpha and beta bands (Fig. S6*A*). For the DMN (seed, LAG; external node, RSFG), the most fMRI-like topography was observed in the theta and alpha bands (Fig. 4). Interestingly, we observed a significant band × node interaction. Stronger correlation with frontal DMN nodes (LMPFC2, LSFS, RMPFC) was observed in theta as compared with alpha or beta bands (Fig. S6*B*). Unambiguously, no long-range gamma band power correlations were obtained even after MCW epoch selection.

Discussion

We report the observation of MEG cortical RSNs. Specifically, MEG power exhibited slow (<2 Hz) spontaneous fluctuations temporally coherent within distributed functional systems with topography resembling well-characterized fMRI RSNs. MEG RSN topography was stronger and more specific with power restricted to lower (theta, alpha, beta) in comparison with higher (gamma) frequencies. Because MEG signals are unambiguously of neural origin, our findings add to accumulating evidence that RSNs are fundamentally a neuronal (5–7, 19) as opposed to a vascular phenomenon (20). There were also important differences between

MEG and fMRI: fMRI networks are largely stationary and bilateral; MEG networks appeared to be strongly nonstationary. Nonstationarity manifested as transient periods of correlation between nodes of a network, with stronger coupling between nodes within hemispheres than across hemispheres.

Spectral Characteristics of MEG RSNs. Spectral analysis of MEG power time series was broadly concordant with previous analyses of band-limited local field potential power (7, 21) in showing a characteristic 1/f-like distribution. Interestingly, total interdependence (17) exhibited a relative local maximum at ~0.1 Hz (Fig. 3*D*) that has been reported also in spontaneous BOLD fluctuations (22). These features raise the possibility that ~0.1-Hz periodicity of cortical hemodynamic signals, originally thought to be intrinsic to the vasculature (23), may actually be of neural origin. Recent computational work has emphasized that 0.1 Hz is a frequency at which the coherence of spontaneous gamma oscillations is optimized given plausible anatomical connectivity, realistic noise, and transmission delays (24).

MEG RSNs were spatially more specific for power within lower in comparison with higher frequencies. Sharper topography was obtained in beta and theta bands for the DAN, and in theta and alpha bands for the DMN (Fig. 4). In the DAN, a network specialized in the control of spatial attention (25), the strength of the correlation was strongest in the alpha band (Fig. S6). This finding agrees with a large body of literature on the association between alpha power modulation, attention states, and cortical information processing (26). It also confirms an association between DAN topography and alpha power fluctuations previously reported in simultaneous EEG-fMRI studies (27, 28). Finally, interference by transcranial magnetic stimulation of activity in FEF and pIPS, core regions of the DAN, has been recently shown to lead to disruption of both spatial attention and alpha rhythms (29).

In the DMN, sharper topography and stronger correlation, especially among prefrontal nodes (LSFS, LMPFC, RMPFC), was observed in the theta as compared with alpha or beta bands (Fig. 4). This finding is consistent with the typical frontal theta power distribution during resting wakefulness (30), and the association of theta activity with working memory (19). Moreover, a recent study reported a trial-to-trial association between theta power changes and BOLD deactivations in MPFC during working memory (31). Finally, a large body of animal and human literature relates hippocampal-prefrontal theta to memory (32), and memory to the DMN (33). It must be noted that gamma-band (27-70 Hz) activity contributed much less to both DMN and DAN RSNs in contrast to that observed with ECoG. Gamma-band LFP strongly relates to BOLD signal responses to stimulation (34), and long-range gamma coherence changes have been reported during visual attention tasks (35). Spontaneous (not task-evoked) long-range interactions in the gamma band have been less well studied, but have been recently reported between visual regions during invasive recordings in animals (6, 7), and between sensory-motor regions of one hemisphere (5) and left and right auditory cortices (7) in humans. In our case, the absence of long-range gamma power correlation is ambiguous. The volume of tissue contributing to LFP signals is small (a few mm^3) compared with the source volume contributing to MEG (a few cm^3). This volume difference is relevant because the spatial scale of synchronous activity tends to be inversely proportional to temporal frequency (36). Thus, relatively poor spatial specificity may, in part, account for a reduced contribution of gamma band LFP power to MEG RSNs. It is possible that stationary large-scale spontaneous interactions will be more evident by considering cross-frequency relationships between fast and slow rhythms (37, 38).

fMRI vs. MEG: Stationarity vs. Nonstationarity. One of the most important findings of this study was that MEG power time series RSNs are markedly nonstationary, which stands in contrast to the fMRI experience. Moreover, the topography of MEG RSNs was more complete, bilateral, and similar to known fMRI topography when this nonstationarity was taken into account by selecting epochs using the MCW algorithm. Epochs of high correlation among a subset of nodes within a network also showed high correlation with other parts of the network. A control experiment involving arbitrarily selected nodes showed that the topography of the nonstationary DAN and DMN was not an artifact of the MCW algorithm (details in *SI Text*).

The discrepancy between electrophysiological and BOLD measures with regard to stationarity is not unexpected. Nonstationarity of the power spectral density of the EEG has been well documented (39). More recently, nonstationary interregional relations in potentials recorded from the surface of the cat cerebral cortex were reported (40). In addition, nonstationary neuronal dynamics on a time scale of seconds has been theoretically simulated in models based on the known anatomical connectivity of the macaque neocortex. These simulations also show a rich temporal structure of cortical electrophysiology at multiple time scales (24, 41, 42). Strong and stationary correlation involving homologous regions of the cerebral cortex is a robust feature of fMRI RSNs. In contrast, MEG power correlation occurs more frequently between regions of the same hemisphere than between regions in opposite hemispheres. This feature has been reported at much greater spatial resolution during bilateral LFP recordings in rat cortex, indicating that spontaneous (not task-evoked) oscillations occur predominantly within one hemisphere and are only loosely coupled between hemispheres (43). This physiology likely reflects the difference between intra- vs. interhemispheric callosal connections that are fewer, more variable in size, and contain a much higher proportion of nonmyelinated slow-conducting fibers (44). These anatomical features imply interhemispheric delays ranging from 5 ms for large myelinated fibers (of which there are relatively few) to 300 ms for thin nonmyelinated fibers (44). Higher temporal variability of interhemispheric MEG power correlations may reflect the larger temporal dispersion in callosal as compared with intrahemispheric pathways where synaptic delays are much shorter (5-10 msec). Typically strong interhemispheric BOLD correlation may thus reflect the fact that neurovascular coupling excludes faster frequencies (nominally, frequencies >1 Hz).

The present findings suggest the possibility that MEG power-based and BOLD RSNs are manifestations of distinct physiological processes within similar if not identical anatomical substrates. The same axonal pathways could just as well support nonstationary as stationary processes. fMRI RSNs might represent functions that are relatively stable, as they strongly overlap with the connectional anatomy (45) and are only weakly modified by major state transitions such as sleep (46) or anesthesia (45). In contrast, MEG RSNs are more transient, and potentially more susceptible to behavioral modulation. Speculatively, under resting conditions, connections supporting more highly synchronized activity (e.g., intrahemispheric with shorter and less variable temporal delays) emerge as robust RSNs. Conversely, regions indirectly or more variably connected (e.g., nonhomologous regions in the two hemispheres) synchronize only transiently. The whole network then becomes more fully engaged in response to environmental stimuli or cognitive states.

Materials and Methods

See *SI Text* for additional details.

Subjects, Procedures, and Acquisition. A total of 13 fMRI (four runs, 6 min each) and MEG (three runs, 5 min each) datasets were acquired in healthy young adult subjects; 10 subjects (mean age 29 ± 6 years, five females) contributed both MEG and fMRI datasets in separate sessions. BOLD time series were acquired using a 1.5 T Siemens Vision scanner (TR = 2.163 s; 3.75 × 3.75 mm in-plane resolution; slice thickness = 8 mm). Neuromagnetic signals were recorded with the MEG system developed at the University of Chieti (47) that includes 153 dc SQUID integrated magnetometers and coregistered to the fMRI data following a procedure described in *SI Text*.

fMRI Analysis. fMRI correlation maps were generated using the pipeline developed at Washington University (3, 11, 13).

MEG Analysis. An extension of the Independent Component Analysis (ICA) algorithm described in ref. 48 was employed to automatically classify and remove artifactual MEG components. Artifact-free MEG signals were reconstituted from the remaining ICs, and source-space current was reconstructed by a weighted minimum-norm least squares (WMNLS) procedure implemented in Curry 6.0 (Neuroscan). This step yielded

$$\mathbf{q}_j(t) = [\,q_{jx}(t) \quad q_{jy}(t) \quad q_{jz}(t)\,]', \qquad [1]$$

the source-space current density vector at voxel *j* at time *t*. Power time series at voxel *j* was computed as

$$p_j(t) = (1/T_p) \int_t^{t+T_p} |\mathbf{q}_j(\tau)|^2 d\tau, \qquad [2]$$

where $T_p = 400$ms. Power time series were reconstructed from wide-band (1-150 Hz) MEG signals and on the basis of $\mathbf{q}_j(t)$ (see [1]) restricted to the theta (3.5–7 Hz), alpha (8-13 Hz), beta (14-25 Hz) and gamma (27-70 Hz) bands. Correlation time series between voxels *j* and *s* (the seed) were computed using the Pearson product moment formula. Thus,

$$r_{sj}(t) = \frac{\int_t^{t+T_r} [p_s(t) - \bar{p}_s][p_j(t+\tau) - \bar{p}_j] d\tau}{\sqrt{\int_t^{t+T_r} [p_s(\tau) - \bar{p}_s]^2 d\tau \int_t^{t+T_r} [p_j(\tau) - \bar{p}_j]^2 d\tau}}, \qquad [3]$$

where T_r is the epoch duration and overbars denote the mean over the appropriate interval. In analyses assuming stationarity, r_{sj} was evaluated and averaged over eight nonoverlapping segments ($T_r \approx 37$sec) within 5-min runs. In analyses taking nonstationarity into account, the maximal correlation window (MCW) algorithm identified epochs of high within-network correlation on which to evaluate $r_{sj}(t)$ ($T_r = 10$sec).

The MCW algorithm accepts as input power time series from four nodes (one of which is the seed) belonging to an fMRI-defined RSN plus one external node. The objective of this algorithm is to identify epochs in which the *least* within-network correlation is above a threshold, whereas the correlation between the seed and one external node is minimal (49).

ACKNOWLEDGMENTS. Funding for this research was provided by the European Community's Seventh Framework Programme (FP7/2007-2013) Grant HEALTH-F2-2008-200728, BrainSynch, and National Institutes of Health Grants NS06833 and MH7192006.

1. Biswal B, Yetkin FZ, Haughton VM, Hyde JS (1995) Functional connectivity in the motor cortex of resting human brain using echo-planar MRI. *Magn Reson Med* 34:537–541.
2. Fox MD, Snyder AZ, Vincent JL, Raichle ME (2007) Intrinsic fluctuations within cortical systems account for intertrial variability in human behavior. *Neuron* 56:171–184.
3. He BJ, et al. (2007) Breakdown of functional connectivity in frontoparietal networks underlies behavioral deficits in spatial neglect. *Neuron* 53:905–918.
4. Logothetis NK, Pauls J, Augath M, Trinath T, Oeltermann A (2001) Neurophysiological investigation of the basis of the fMRI signal. *Nature* 412:150–157.
5. He BJ, Snyder AZ, Zempel JM, Smyth MD, Raichle ME (2008) Electrophysiological correlates of the brain's intrinsic large-scale functional architecture. *Proc Natl Acad Sci USA* 105:16039–16044.
6. Shmuel A, Leopold DA (2008) Neuronal correlates of spontaneous fluctuations in fMRI signals in monkey visual cortex: Implications for functional connectivity at rest. *Hum Brain Mapp* 29:751–761.
7. Nir Y, et al. (2008) Interhemispheric correlations of slow spontaneous neuronal fluctuations revealed in human sensory cortex. *Nat Neurosci* 11:1100–1108.
8. Shmuel A, Augath M, Oeltermann A, Logothetis NK (2006) Negative functional MRI response correlates with decreases in neuronal activity in monkey visual area V1. *Nat Neurosci* 9:569–577.
9. Hamalainen M, Hari R, Llomniemi RJ, Knuutila J, Lounasmaa OV (1993) Magneto-encephalography, theory, instrumentation, and applications to noninvasive studies of the working brain. *Rev Mod Phys* 65:413–497.
10. Shulman GL, et al. (1997) Common blood flow changes across visual tasks: II. Decreases in cerebral cortex. *J Cogn Neurosci* 9:648–663.
11. Fox MD, et al. (2005) The human brain is intrinsically organized into dynamic, anticorrelated functional networks. *Proc Natl Acad Sci USA* 102:9673–9678.
12. Fox MD, Zhang D, Snyder AZ, Raichle ME (2009) The global signal and observed anticorrelated resting state brain networks. *J Neurophysiol* 101:3270–3283.
13. Fox MD, Corbetta M, Snyder AZ, Vincent JL, Raichle ME (2006) Spontaneous neuronal activity distinguishes human dorsal and ventral attention systems. *Proc Natl Acad Sci USA* 103:10046–10051.
14. Johnston JM, et al. (2008) Loss of resting interhemispheric functional connectivity after complete section of the corpus callosum. *J Neurosci* 28:6453–6458.
15. Friston KJ, et al. (1998) Event-related fMRI: Characterizing differential responses. *Neuroimage* 7:30–40.
16. Glover GH (1999) Deconvolution of impulse response in event-related BOLD fMRI. *Neuroimage* 9:416–429.
17. Schelter B, Winterhalder M, Timmer J (2006) *Handbook of Time Series Analysis: Recent Theoretical Developments and Applications* (Wiley-VCH, Berlin).
18. Buzsáki G, Draguhn A (2004) Neuronal oscillations in cortical networks. *Science* 304: 1926–1929.
19. Meltzer JA, Negishi M, Mayes LC, Constable RT (2007) Individual differences in EEG theta and alpha dynamics during working memory correlate with fMRI responses across subjects. *Clin Neurophysiol* 118:2419–2436.
20. Shmueli K, et al. (2007) Low-frequency fluctuations in the cardiac rate as a source of variance in the resting-state fMRI BOLD signal. *Neuroimage* 38:306–320.
21. Leopold DA, Murayama Y, Logothetis NK (2003) Very slow activity fluctuations in monkey visual cortex: Implications for functional brain imaging. *Cereb Cortex* 13:422–433.
22. Purdon PL, Weisskoff RM (1998) Effect of temporal autocorrelation due to physiological noise and stimulus paradigm on voxel-level false-positive rates in fMRI. *Hum Brain Mapp* 6:239–249.
23. Mayhew JE, et al. (1996) Cerebral vasomotion: A 0.1-Hz oscillation in reflected light imaging of neural activity. *Neuroimage* 4:183–193.
24. Deco G, Jirsa V, Mcintosh AR, Sporns O, Kotter R (2009) Key role of coupling, delay, and noise in resting brain fluctuations. *Proc Natl Acad Sci USA* 106:10302–10307.
25. Corbetta M, Shulman GL (2002) Control of goal-directed and stimulus-driven attention in the brain. *Nat Rev Neurosci* 3:201–215.
26. Nunez P (1995) *Neocortical Dynamics and Human EEG Rhythms* (Oxford Univ Press, New York).
27. Laufs H, et al. (2003) Electroencephalographic signatures of attentional and cognitive default modes in spontaneous brain activity fluctuations at rest. *Proc Natl Acad Sci USA* 100:11053–11058.
28. Mantini D, Perrucci MG, Del Gratta C, Romani GL, Corbetta M (2007) Electrophysiological signatures of resting state networks in the human brain. *Proc Natl Acad Sci USA* 104:13170–13175.
29. Capotosto P, Babiloni C, Romani GL, Corbetta M (2009) Frontoparietal cortex controls spatial attention through modulation of anticipatory alpha rhythms. *J Neurosci* 29:5863–5872.
30. Srinivasan R, Winter WR, Nunez PL (2006) Source analysis of EEG oscillations using high-resolution EEG and MEG. *Prog Brain Res* 159:29–42.
31. Scheeringa R, et al. (2009) Trial-by-trial coupling between EEG and BOLD identifies networks related to alpha and theta EEG power increases during working memory maintenance. *Neuroimage* 44:1224–1238.
32. Hasselmo ME, Eichenbaum H (2005) Hippocampal mechanisms for the context-dependent retrieval of episodes. *Neural Netw* 18:1172–1190.
33. Buckner RL, Andrews-Hanna JR, Schacter DL (2008) The brain's default network: Anatomy, function, and relevance to disease. *Ann N Y Acad Sci* 1124:1–38.
34. Goense JB, Logothetis NK (2008) Neurophysiology of the BOLD fMRI signal in awake monkeys. *Curr Biol* 18:631–640.
35. Gregorious G, Gotts S, Zhou H, Desimone R (2009) High-frequency, long-range coupling between prefrontal and visual cortex during attention. *Science* 29:1207–1210.
36. Bullock TH, et al. (1995) Temporal fluctuations in coherence of brain waves. *Proc Natl Acad Sci USA* 92:11568–11572.
37. Mazaheri A, Nieuwenhuis IL, van Dijk H, Jensen O (2009) Prestimulus alpha and mu activity predicts failure to inhibit motor responses. *Hum Brain Mapp* 30:1791–1800.
38. de Lange FP, Jensen O, Bauer M, Toni I (2008) Interactions between posterior gamma and frontal alpha beta oscillations during imagined actions. *Front Hum Neurosci* 2:7.
39. Zhan Y, Halliday D, Jiang P, Liu X, Feng J (2006) Detecting time-dependent coherence between non-stationary electrophysiological signals—a combined statistical and time-frequency approach. *J Neurosci Methods* 156:322–332.
40. Popa D, Popescu AT, Paré D (2009) Contrasting activity profile of two distributed cortical networks as a function of attentional demands. *J Neurosci* 29:1191–1201.
41. Honey CJ, Kötter R, Breakspear M, Sporns O (2007) Network structure of cerebral cortex shapes functional connectivity on multiple time scales. *Proc Natl Acad Sci USA* 104:10240–10245.
42. Ghosh A, Rho Y, McIntosh AR, Kötter R, Jirsa VK (2008) Noise during rest enables the exploration of the brain's dynamic repertoire. *PLOS Comput Biol* 4:e1000196.
43. MacDonald KD, Brett B, Barth DS (1996) Inter- and intra-hemispheric spatiotemporal organization of spontaneous electrocortical oscillations. *J Neurophysiol* 76:423–437.
44. Ringo JL, Doty RW, Demeter S, Simard PY (1994) Time is of the essence: A conjecture that hemispheric specialization arises from interhemispheric conduction delay. *Cereb Cortex* 4:331–343.
45. Vincent JL, et al. (2007) Intrinsic functional architecture in the anaesthetized monkey brain. *Nature* 447:83–86.
46. Horovitz SG, et al. (2008) Low frequency BOLD fluctuations during resting wakefulness and light sleep: A simultaneous EEG-fMRI study. *Hum Brain Mapp* 29:671–682.
47. Della Penna S, et al. (2000) Biomagnetic systems for clinical use. *Philos Mag B* 80:937–948.
48. Hironaga N, Ioannides AA (2007) Localization of individual area neuronal activity. *Neuroimage* 34:1519–1534.
49. Hu TC, Kahng AB, Tsao CWA (1995) Old bachelor acceptance: A new class of non-monotone threshold accepting methods. *ORSA Journal on Computing* 7:417–425.